

# The Accretion and Cooling of Preheated Gas in Dark Matter Halos

Yu Lu<sup>1\*</sup>, H.J. Mo<sup>1</sup>

<sup>1</sup> *Department of Astronomy, University of Massachusetts, Amherst MA 01003-9305, USA*

## ABSTRACT

We use a one-dimensional hydrodynamical code to investigate the effects of preheating on gas accretion and cooling in cold dark matter halos. In the absence of radiative cooling, preheating reduces the amount of gas that can be accreted into a halo, and the accreted gas fraction is determined by the ratio of the initial specific entropy of the gas to the virial entropy of the halo,  $S_{\text{ph}}/S_{\text{v}}$ . In the presence of radiative cooling, preheating affects the gas fraction that can cool in two different ways. For small halos with masses  $M < 10^{12} h^{-1} M_{\odot}$ , preheating suppresses gas accretion, but most of the accreted gas can cool. For more massive halos, preheating affects the cold gas fraction not only by reducing the amount of accreted gas, but also by reducing the cooling efficiency. For both small and massive halos, gas cooling is delayed by preheating if the halo gas is assumed to be a single-phase medium. However, if the halo gas is assumed to be a multi-phase medium, cooling can occur over a wider range of redshifts. Unlike in a single-phase medium where cooling is inside-out, gas cooling in a preheated multi-phase medium can occur simultaneously over a wide range of radii. As examples, two specific preheating cases are investigated. In the first case, the preheating specific entropy is assumed to be proportional to the virial entropy of the halo,  $S_{\text{ph}} \propto S_{\text{v}}$ , as expected from AGN feedback. Such preheating effectively suppresses radiative cooling in halos with  $M > 10^{13} h^{-1} M_{\odot}$ , but has little effect on smaller halos. We suggest that this may be the reason why the stellar mass function of galaxies breaks sharply at the massive end. Such preheating also helps create the hot diffused halos within which the “radio mode” feedback of AGNs can act effectively. In the second case, the intergalactic medium is assumed to be warm. Here the total amount of gas that can cool in a halo scales with halo mass as  $\propto M^2$ , as would be required to match the observed stellar- and HI-mass functions in the current CDM model at the small mass end.

**Key words:** galaxies: formation — hydrodynamics — methods: numerical

## 1 INTRODUCTION

According to the current theory of structure formation, galaxies are believed to form in cold dark matter (CDM) halos that are virialized clumps of CDM formed through gravitational instability from initial density perturbations in the early universe. In this scenario, the problem of galaxy formation can be divided roughly into two parts: (1) the formation of CDM halos in the cosmic density field, and (2) the accretion and cooling of gas into dark matter halos to form stars and the structures of luminous galaxies. The buildup of dark matter halos is now fairly well understood using both analytic models (e.g. Press & Schechter 1974; Bond et al. 1991; Sheth, Mo & Tormen 2001) and  $N$ -body simulations (e.g. Navarro, Frenk & White 1996; Jing & Suto

2000; Moore et al. 1998; Zhao et al. 2003a, b; Wechsler et al. 2002). However, how gas cools and assembles to form the luminous part of a galaxy is still an open question.

The pioneering work by Binney (1977), Rees & Ostriker (1977) and Silk (1977) assumed that the gas in a dark matter halo is heated by shocks as it collapses into dark matter halos. The heated gas then cools via radiative processes, and forms stars in the centers of dark halos. This assumption has been combined with the halo population predicted by CDM models to make predictions for the properties of the galaxy population, such as the luminosity function, the colour distribution, etc (White & Rees 1978; White & Frenk 1991). With modern computational facilities and numerical codes, many of the processes in galaxy formation can be studied in more detail with numerical simulations (e.g., Katz & Gunn 1991; Cen & Ostriker 1992; Springel & Hernquist 2003).

Despite the progress made so far, galaxy formation re-

\* E-mail: luyu@astro.umass.edu

mains one of the most challenging problems in astrophysics. One of the long-standing problems in the CDM scenario of galaxy formation is to match the halo mass function with the luminosity function of galaxies. The galaxy luminosity function has a characteristic shape that is very different from the halo mass function. The faint end slope of the galaxy luminosity function is significantly shallower than the halo mass function at the low-mass end. Also, the galaxy luminosity function has an abrupt break at the bright end, while such decline in the halo mass function occurs at a mass that corresponds to a much lower abundance (Yang et al. 2003). Furthermore, as shown in Yang et al. (2005), the relation between the luminosity of the central galaxy in a halo and the halo mass is strongly nonlinear at both the low-mass and high-mass ends. These results imply that the efficiency of star formation must be suppressed in both low-mass and high-mass halos.

Various suggestions have been made to explain the dependence of star formation efficiency on halo mass. For massive halos, it has been suggested that the low star formation efficiency is a result of the inefficient gas cooling. Thoul & Weinberg (1995) studied gas cooling in massive halos in considerable detail and found that a significant amount of gas can still cool in such halos, although the cooling efficiency is lower than that in lower mass halos. Thus, radiative cooling alone may not be able to explain the bright-end behavior in the galaxy luminosity function. For low mass halos, suggestions have been made that heating by the UV background and/or supernova explosions associated with star formation may suppress gas cooling and hence the star formation efficiency. However, heating by the UV background is effective only in small halos with masses  $M < 10^{10} h^{-1} M_{\odot}$  at low redshift (Quinn et al. 1996; Gnedin et al. 2000; Hoefl et al. 2006) and its effect is reduced by self-shielding at high redshifts (Dijkstra et al. 2004). Heating by supernova explosions may also be ineffective because of the development of Rayleigh-Taylor instabilities in the interstellar medium (e.g. Mac Low & Ferrara 1999; Strickland & Stevens 2000).

One important process that can prevent gas from cooling too fast in dark matter halos is preheating (e.g. Mo & Mao 2002; Oh & Benson 2003; Scannapieco & Oh 2004; Mo et al. 2005). In this scenario, the intergalactic gas is assumed to be heated to some finite entropy before it is accreted into dark matter halos. This will affect how gas is accreted into dark matter halos (e.g. Mo & Mao 2002; van den Bosch, Abel & Hernquist 2003), and the distribution, thermal state and radiative cooling of the accreted gas. In this paper, we use 1-D simulations to study in detail the effects of preheating on galaxy formation in dark matter halos. We find a number of scaling relations that are useful to understand and to model galaxy formation in preheated media. Furthermore, we consider two realistic cases of preheating and study their consequences on the formation of the central galaxies in dark matter halos. In one, preheating is assumed to be generated by the energy feedback of AGNs. We show that such preheating can effectively suppress gas cooling in halos more massive than  $\sim 10^{13} M_{\odot}$ . In the second case, we consider a constant, relatively low entropy floor and study its effect on mass accretion and cooling in low-mass halos. This model is motivated by the fact that low-mass halos at low redshift may be surrounded by a warm intergalactic medium generated by gravitational pancaking (Mo et al. 2005). Our

results show that the cold gas fraction in small dark matter halos can be significantly reduced in such a warm medium.

This paper is organized as follows. We briefly describe the numerical scheme of our 1-D hydrodynamical code and simulation models in Section 2. In Section 3, we show adiabatic simulation results and discuss the effects of preheating on gas accretion. In Section 4, we study the cooling of preheated media in halos of different masses using both single-phase and multi-phase simulations. We implement our simulations to study the two particular preheating models in Section 5. Further discussion and a summary of our results are given in Section 6.

## 2 MODEL AND SIMULATION

In this paper, we use 1-Dimensional Lagrangian hydrodynamical simulations to study the accretion and cooling of gas in dark matter halos. In these simulations, the mass distribution is assumed to be spherically symmetric, and the radial distributions of the dark matter and gas are represented by spherical shells, each of which contains a certain amount of mass. The motions of the dark matter shells are followed with the same 1-d code as described in Lu et al. (2006). In what follows, we describe how we simulate the evolution of the gas component.

### 2.1 Hydrodynamics and thermodynamics

We treat the gas component as fluid, so the motion is governed by the following set of equations:

$$\frac{d\rho_g}{dt} + \rho_g \nabla \cdot v_g = 0; \quad (1)$$

$$\frac{dv_g}{dt} = -\frac{\nabla p}{\rho_g} - \nabla \Phi; \quad (2)$$

$$\frac{du}{dt} = \frac{p}{\rho_g^2} \frac{d\rho_g}{dt} + \frac{\Gamma - \Lambda}{\rho_g}; \quad (3)$$

$$p = (\gamma - 1)\rho_g u. \quad (4)$$

These are the continuity equation, the momentum equation, the energy equation, and the equation of state, respectively. In these equations,  $\rho_g$ ,  $p$  and  $u$  are, respectively, the density, pressure and specific thermal energy of the gas;  $v_g$  is the fluid velocity;  $\Phi$  is the gravitational potential;  $\gamma$  is the adiabatic index (assumed to be 5/3 in the following);  $\Gamma$  and  $\Lambda$  are the specific heating and cooling rates. For spherical symmetry, the continuity equation and momentum equation can be rewritten as

$$dm_g = 4\pi r_g^2 \rho_g dr_g; \quad (5)$$

$$\frac{dv_g}{dt} = -4\pi r_g^2 \frac{dp}{dm_g} - \frac{GM(< r_g)}{r_g^2}, \quad (6)$$

where  $M(< r_g)$  is the total mass (including dark matter) enclosed by a sphere with radius  $r_g$  and  $G$  is gravitational constant. Note that the specific thermal energy of the gas can change not only by cooling and heating but also by adiabatic expansion and compression. Instead of the energy equation, one may choose to integrate the entropy equation. We define the specific entropy as

$$S = \frac{T}{n^{2/3}}, \quad (7)$$

where  $T$  is the temperature, and  $n$  is the particle number density of the gas. We can then write the equation of state as

$$p = A\rho_g^\gamma, \quad (8)$$

where the adiabat  $A$  is related to  $S$  as

$$A = \frac{k}{\mu m_H} \cdot S, \quad (9)$$

where  $k$  is the Boltzmann constant,  $\mu$  is the mean molecular weight and  $m_H$  is the mass of a hydrogen atom. The adiabat can be changed when the gas is heated or cools, or as it is shocked. We can therefore write

$$dA = \frac{(\gamma - 1)dQ}{\rho_g^{\gamma-1}}; \quad (10)$$

$$dQ = dW_{\text{shock}} + dQ_{\text{hc}}, \quad (11)$$

where  $dW_{\text{shock}}$  is the work done by shock, and  $dQ_{\text{hc}}$  is the heat due to other cooling and heating processes.

In most of the simulations presented in this paper, atomic radiative cooling is incorporated using the cooling function given in Katz, Weinberg & Hernquist (1996). We assume the gas has a primordial abundance, i.e. 76% of the mass is in hydrogen, 24% is in helium, and there are no heavier elements. The atomic cooling processes considered here work only for temperature above  $\sim 10^4\text{K}$ . We calculate the abundance of different ionic species as a function of density and temperature assuming ionization equilibrium. Since the shock front is thin compared to all the length scales of interest, the mass of gas involved in the shock front is only a small fraction. Following Thoul and Weinberg (1995), we ignore cooling in the shock front.

## 2.2 Numerical scheme

We use the Lagrangian finite-difference scheme of Bowers & Wilson (1991) to follow the evolution of gas shells. In this scheme, phase space quantities, such as positions and velocities are zone-edge-centered, while thermodynamic quantities, such as pressure, density and entropy/energy are zone-centered. In what follows, subscripts denote the index/position of gas shells. The acceleration of the  $i$ th gas shell is

$$a_i = -4\pi r_i^2 \frac{p_{i+} - p_{i-}}{m_i} + g_i, \quad (12)$$

where  $p_{i+}$  and  $p_{i-}$  are the pressures of the gas at the outer and inner sides of the shell,  $m_i$  is mass of the gas shell, and  $g_i$  is gravitational acceleration.

The time integration is carried out by the DKD (drift-kick-drift) leap-frog algorithm:

$$r_i^{n+1/2} = r_i^n + \frac{1}{2}v_i^n dt^n; \quad (13)$$

$$v_i^{n+1} = v_i^n + a_i^{n+1/2} dt^n; \quad (14)$$

$$r_i^{n+1} = r_i^{n+1/2} + \frac{1}{2}v_i^{n+1} dt^n, \quad (15)$$

in which superscripts denote the current time step. Once the integration is carried out to the  $n$ th step, we can calculate the gas density between every two neighboring shells:

$$\rho_{i-}^n = \frac{3m_i}{4\pi [(r_i^n)^3 - (r_{i-1}^n)^3]}. \quad (16)$$

During this time step, the change of adiabat is

$$\Delta A_{i-}^n = \frac{\gamma - 1}{(\rho_{i-}^n)^{\gamma-1}} (\Delta W_{\text{shock},i-}^n + \Delta Q_{\text{hc},i-}^n), \quad (17)$$

where the work done by the shock is given by

$$\Delta W_{\text{shock},i-}^n = \frac{p_{\text{shock},i-}^n \cdot \Delta V_{i-}^n}{m_{i-}} = p_{\text{shock},i-}^n \cdot \left( \frac{1}{\rho_{i-}^{n+1}} - \frac{1}{\rho_{i-}^n} \right). \quad (18)$$

Here  $p_{\text{shock}}$  is equivalent to the shock pressure using an artificial viscosity technique (Richtmyer & Morton 1967; Thoul & Weinberg 1995):

$$p_{\text{shock},i-} = -\frac{2\alpha}{1/\rho_{i-}^{n+1} + 1/\rho_{i-}^n} \cdot |v_i^{n+1/2} - v_{i-1}^{n+1/2}| \times (v_i^{n+1/2} - v_{i-1}^{n+1/2}), \quad (19)$$

if  $v_i^{n+1/2} - v_{i-1}^{n+1/2} < 0$ , and  $p_{\text{shock},i-} = 0$  otherwise. Following Thoul & Weinberg (1995), we choose  $\alpha = 4$ . Our tests show that the results are not sensitive to the value of this parameter. The other entropy source term comes from radiative cooling,

$$\Delta Q_{\text{hc},i-}^n = -\frac{\Lambda_{i-}^n}{\bar{\rho}_{i-}^n} \Delta t^{n+1/2}, \quad (20)$$

where  $\bar{\rho}_{i-}^n = \sqrt{\rho_{i-}^n \rho_{i-}^{n+1}}$  is the mean density of the gas shells during the  $n$ th time step. The advanced adiabat at the next time step is

$$A_{i-}^{n+1} = A_{i-}^n + \Delta A_{i-}^n. \quad (21)$$

Other thermal quantities at the new time step are derived as follows:

$$p_{i-}^{n+1} = A_{i-}^{n+1} (\rho_{i-}^{n+1})^\gamma; \quad (22)$$

$$u_{i-}^{n+1} = \frac{A_{i-}^{n+1}}{\gamma - 1} (\rho_{i-}^{n+1})^{\gamma-1}. \quad (23)$$

We ignore radiative cooling on the shell front, at which  $v_i^{n+1/2} - v_{i-1}^{n+1/2} < 0$  and  $v_i \gg C_{s,i-}$ , where  $C_{s,i-} = \sqrt{\gamma p_{i-} / \rho_{i-}}$  is the adiabatic sound speed for the shell.

When a gas shell cools to a temperature below  $10^4\text{K}$ , the gas in the shell is considered to be cold. Since we do not include any cooling processes below this temperature, the cold gas is assumed to retain a temperature of  $10^4\text{K}$  until it flows into the center of the halo, where we drop the cold gas out of the gas component. Once a gas shell is dropped out, we do not trace its dynamical evolution anymore. Instead, we put the gas in a central exponential disk with a scale-length  $r_d = \frac{0.05}{\sqrt{2}} r_v$  (Mo, Mao & White 1998), where  $r_v$  is the virial radius of the halo at  $z = 0$ . The cold gas disk is assumed to be a rigid object, and its gravity is included in the subsequent evolution of the other mass shells.

Each time step of the integration is controlled to be smaller than any of the important timescales: the dynamical, the Courant, and the cooling timescales,

$$\Delta t_{\text{dyn}} = \min_i \left\{ c_d \sqrt{\frac{5r_i^3}{2GM_i}} \right\}, \quad (24)$$

$$\Delta t_{\text{Cour}} = \min_i \left\{ c_C \left| \frac{r_i - r_{i-1}}{C_s} \right| \right\}, \quad (25)$$

$$\Delta t_{\text{cool}} = \min_i \left\{ c_c \left| \frac{u_i \rho_i}{\Lambda_i} \right| \right\}, \quad (26)$$

where  $c_d$ ,  $c_C$  and  $c_c$  are safety parameters. Moreover, in order to avoid shell crossing, we have an additional time step control,

$$\Delta t_{\text{vel}} = \min_i \left\{ c_v \left| \frac{r_i - r_{i-1}}{v_i - v_{i-1}} \right| \right\}, \quad (27)$$

where  $c_v$  is again a safety parameter. In practice, the time step is chosen to be the minimum of all the above time steps,

$$dt = \min\{dt_{\text{dyn}}, dt_{\text{Cour}}, dt_{\text{cool}}, dt_{\text{vel}}\}. \quad (28)$$

The safety parameters are taken to be  $c_d = 0.01$ ,  $c_C = 0.2$ ,  $c_c = 0.1$ , and  $c_v = 0.05$ , as suggested by Thoul & Weinberg (1995).

The numerical code was tested against idealized problems with analytical solutions, such as the Sedov solution and the self-similarity models of Bertschinger (1983). The code also reproduces the results of Thoul & Weinberg (1995).

### 2.3 Initial conditions

The simulation starts from an initial condition, which specifies the position, velocity and other properties of each shell at a high redshift,  $z = z_i$ . We set up our initial condition based on the mass accretion histories (MAHs) of dark matter halos.  $N$ -body simulations show that the mass accretion histories of CDM halos have some universal behaviors (e.g. Wechsler et al. 2002; Zhao et al. 2003a; b), and can be described by a simple functional form,

$$M(a) = M_0 \exp \left[ -2a_c \left( \frac{a_0}{a} - 1 \right) \right], \quad (29)$$

where  $a$  is the expansion scale factor,  $a_c$  is the scale factor corresponding to the formation time of the halo, and  $M_0$  is mass of the halo at the observation time  $a_0$  (Wechsler et al. 2002). Note that  $a_c$  is the single free parameter.

Once the mass accretion history is specified, we can use it to determine the density profile of the initial perturbation. In an expanding universe, a mass shell turns around and then collapses at a time that depends on the initial overdensity within the mass shell. Based on a spherical collapse model, a mass shell collapses at a time when the linear overdensity reaches  $\approx 1.686$ . Thus, the initial over-density within a mass shell that collapses at a redshift  $z$  can be written as

$$\delta_i(M) = 1.686 \frac{D(z_i)}{D(z)}, \quad (30)$$

where  $D(z)$  is the linear growth factor, and  $M$  is the mass within the mass shell. The mass  $M$  is related to the initial radius  $r_i$  of the mass shell by

$$r_i = \left[ \frac{M}{\frac{4}{3}\pi\bar{\rho}(z_i)[1 + \delta_i(M)]} \right]^{1/3}, \quad (31)$$

where  $\bar{\rho}_i = \rho_{\text{crit},0} \cdot \Omega_M \cdot (1 + z_i)^3$  is the mean matter density at redshift  $z_i$ ,  $\rho_{\text{crit},0}$  is the critical density of the universe at the present time, and  $\Omega_M$  is the matter density parameter. For a given cosmology and halo mass accretion history, the above relations allow us to specify  $\delta_i$  as a function  $r_i$ .

The initial velocity of each mass shell has two components, the Hubble expansion  $v_i = r_i H(z_i)$ , and the peculiar velocity owing to the density perturbation:

$$\mathbf{v} = \frac{2f}{3H\Omega_M} \mathbf{g}, \quad (32)$$

where  $\mathbf{g}$  is the peculiar gravitational acceleration,

$$\mathbf{g}(\mathbf{x}) = G\rho_b a \int d^3x' \delta(\mathbf{x}', t) (\mathbf{x} - \mathbf{x}') / |\mathbf{x}' - \mathbf{x}|^3, \quad (33)$$

and  $f = d \ln D(z) / d \ln(1 + z)$ , with all the quantities evaluated at the initial redshift  $z_i$ . We choose  $z_i = 200$ , and the initial temperature of gas shells is set to be the CMB temperature at this epoch.

Our simulations cover a large range of halo mass, from  $10^{10}$  to  $10^{15} h^{-1} M_\odot$ . In hierarchical structure formation, the value of  $a_c$  is correlated with halo mass. In our simulations, we use the typical value of  $a_c$  for halos of a given mass. The parameters of the halo models are described in Table 1. As in Lu et al. (2006), particles accreted before  $z_c$  are assumed to have isotropic velocities, so that the final dark halos have the Navarro, Frenk & White profiles (Navarro et al. 1996, 1997).

In all the simulations, we assume  $\Omega_M = 0.3$  and  $\Omega_\Lambda = 0.7$  at the present time. We fix the baryon fraction to be  $f_b = 0.17$  for our fiducial model, but vary this parameter in some of our simulations. We use  $5 \times 10^4$  shells of the same mass for the dark matter, and 500 equal-mass shells for the gas component. To avoid a numerical instability caused by dark matter shell-crossing, the mass of each dark matter shell is chosen to be smaller than that of the gas shell. Our tests with higher resolutions show that our resolution ensures numerical convergence.

### 3 ACCRETION BY DARK MATTER HALOS IN A PREHEATED MEDIUM

In this section, we present simulation results that neglect radiative cooling. First, we consider models in which the intergalactic medium is cold. During the formation of a dark matter halo, gas is accreted and shocked. In the absence of radiative cooling, the temperature of the post-shock gas is roughly given by the in-fall kinetic energy of the gas:

$$T_{ps} = \frac{3\mu m_H v_s^2}{16k}, \quad (34)$$

where the shock velocity  $v_s$  is approximately the virial velocity of the halo at the time in consideration. Since the gravitational potential of the halo is established at an early stage of halo formation, the virial velocity does not change much at later times. This is the main reason for the rather flat temperature profiles shown in the left panel of Figure 1. Note that, as the halo mass increases with time, the radius within which the gas is shock heated also increases.

The right panel of Figure 1 shows the evolution of the specific entropy profile. The specific entropy of the accreted gas increases with radius, because the density of shocked gas is lower at larger radius. The entropy profile is roughly a power-law and shows a self-similar behavior. Indeed, it scales the radius  $r$  in units of the present virial radius, and scales the specific entropy in units of the ‘‘virial entropy’’, defined as

$$S_v = \frac{T_v}{n_v^{2/3}}, \quad (35)$$

**Table 1.** Halo models

$M$ ( $h^{-1} M_{\odot}$ )	$10^{10}$	$10^{11}$	$10^{12}$	$10^{13}$	$10^{14}$	$10^{15}$
$a_c$	0.2	0.23	0.3	0.4	0.6	0.8
$z_c$	4.0	3.3	2.3	1.5	0.67	0.25

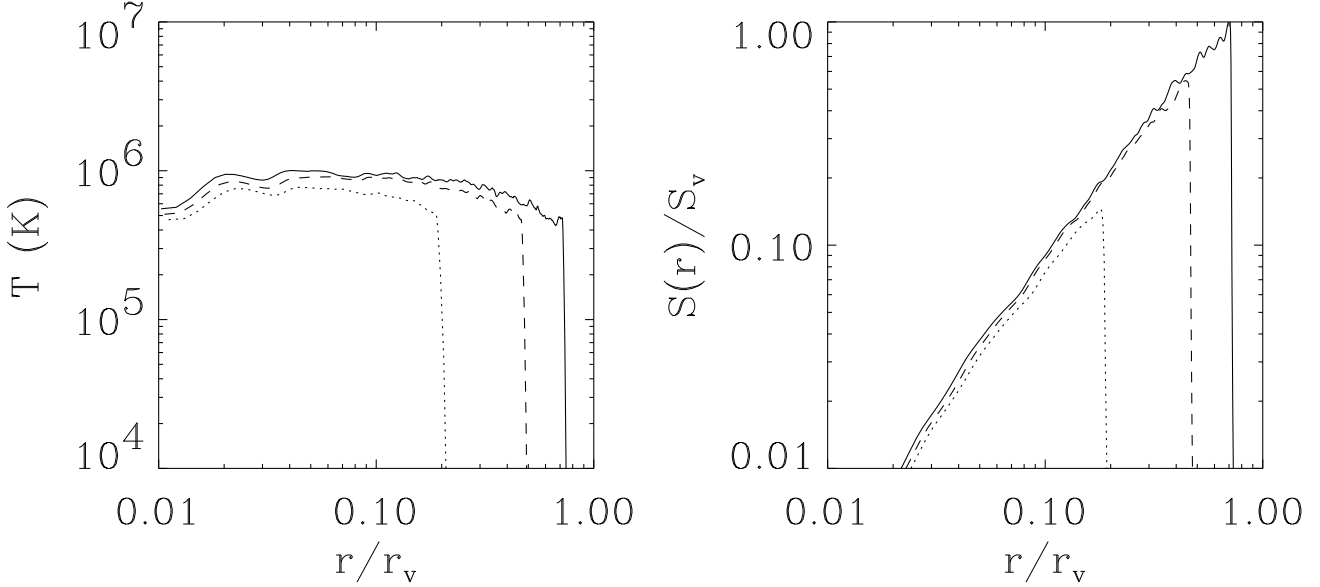


**Figure 1.** The evolution of temperature (left panel) and normalized entropy profile (right panel) of a  $M = 10^{12} h^{-1} M_{\odot}$  halo in the absence of preheating. The dotted, dashed, and solid curves correspond to  $z = 3, 1.5$  and  $0.85$ , respectively. The radius is scaled to the virial radius of the halo at  $z = 0$ . The sharp breaks correspond to the shock fronts.

where  $n_v$  is the mean particle density within the virialized halo, the entropy profiles for halos of different masses all obey:

$$\frac{S(r)}{S_v} = \left(\frac{r}{r_v}\right)^{\alpha}, \quad (36)$$

with  $\alpha \sim 1.3$ , as shown in Figure 2. This result is consistent with the analytical work of Tozzi & Norman (2001), but the slope is steeper than the observed entropy profiles of nearby cooling flow clusters (Piffaretti et al 2005), which have  $\alpha \sim 0.95$ . As we shall see, radiative cooling changes the entropy profile.

Next, we consider cases where the gas is preheated to a finite entropy before it is accreted into dark matter halos. In the simulations, the preheating entropy is gradually added into gas shells at early epochs, from  $z = 100$  to  $10$ , to make the numerical calculations stable. Here again we neglect radiative cooling. In Figure 3 we show the entropy profiles for cases with different initial entropies. One can clearly see the imprint of the initial entropy. The entropy profile is flat at small radii, with an amplitude comparable to the initial entropy, since the entropy generated by accretion shocks is smaller than the initial entropy at small radii. Since the entropy generated by shocks increases with

radius, the entropy profile will eventually be dominated by shock generation and follow that of no preheating case. This transition occurs roughly at the radius where the shock entropy equals to the preheating entropy. The final entropy profile can, therefore, roughly be described by

$$S(r) = \begin{cases} S_{\text{ph}} & \text{if } r < r_t; \\ S^0(r) & \text{if } r \geq r_t, \end{cases} \quad (37)$$

where  $S_{\text{ph}}$  is the preheating entropy,  $S^0(r)$  is the entropy expected from cold accretion, and  $r_t$  is the radius at which  $S^0 = S_{\text{ph}}$ . Since  $S^0(r)/S_v$  is roughly a scale-free function of  $r/r_v$ , the characteristic radius  $r_t$ , expressed in units of  $r_v$ , is determined by  $S_{\text{ph}}/S_v$ . Hence, the effect of preheating in adiabatic accretion is almost entirely determined by the ratio  $S_{\text{ph}}/S_v$ .

As expected, preheating reduces the amount of gas that accretes into a halo. In Figure 4 we show the ratio of  $f_g(S_{\text{ph}})/f_g(0)$  as a function of  $S_{\text{ph}}/S_v$ , where  $f_g(S_{\text{ph}})$  is the ratio between the mass of accreted gas and the halo mass, and  $f_g(0)$  is the corresponding ratio for the non-preheating model. As one can see, the  $f_g(S_{\text{ph}})/f_g(0) - S_{\text{ph}}/S_v$  relation is independent of both the halo mass and of the initial baryonic fraction. The relation can be well described by

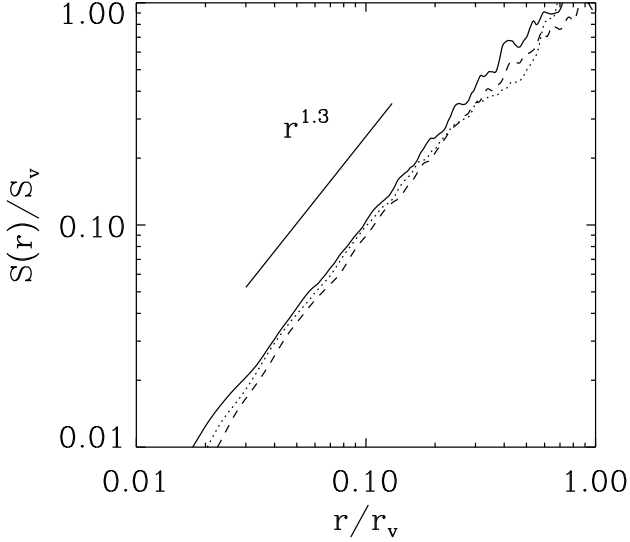


**Figure 2.** The normalized specific entropy profiles for halos of different masses at  $z = 0$ . The solid, dashed and dotted curves are for halos with masses of  $10^{10}$ ,  $10^{12}$  and  $10^{14} h^{-1} M_{\odot}$ , respectively. We scale the radius to the virial radius,  $r_v$ , and scale the specific entropy to the virial entropy,  $S_v$ , as defined in the text.

$$f_g/f_g(0) = \frac{1}{\left[1 + \left(\frac{S_{\text{ph}}/S_v}{0.8}\right)^3\right]^{1/2}}. \quad (38)$$

This relation shows that the reduction in the accreted gas becomes important when the preheating entropy is comparable to or larger than  $S_v$ . For  $S_{\text{ph}} \gg S_v$ ,  $f_g/f_g(0) \propto (S_{\text{ph}}/S_v)^{-3/2}$ , and if  $S_{\text{ph}} = \text{constant}$  then  $f_g/f_g(0)$  is proportional to the halo mass,  $M$ . In the last relation we assumed the virial density  $n_v$  is independent of the halo mass. This relation is similar to that obtained by Mo & Mao (2002) based on a simple analytical model.

#### 4 COOLING OF PREHEATED GAS IN DARK MATTER HALOS

Since preheating modifies the distribution of the accreted gas in dark halos, it can change the gas cooling rate (Mo & Mao 2002). In this section, we explore how preheating affects gas cooling in different halos.

##### 4.1 Cooling in single-phase media

To begin, we assume that the accreted gas in a dark halo has a single-phase. Thus, at any given time, each gas shell has a unique temperature and density. In the simulation, the accreted gas dissipates its thermal energy via radiative cooling, and its temperature drops. We consider the gas to be in a cold component when its temperature drops below  $10^4 \text{K}$ . To characterize the efficiency of cooling, we study the fraction of the accreted gas that is in the cold component at  $z = 0$ . For simulations with preheating, we denote the total cold gas mass and the total accreted gas mass by  $M_{\text{cool}}(S_{\text{ph}})$  and

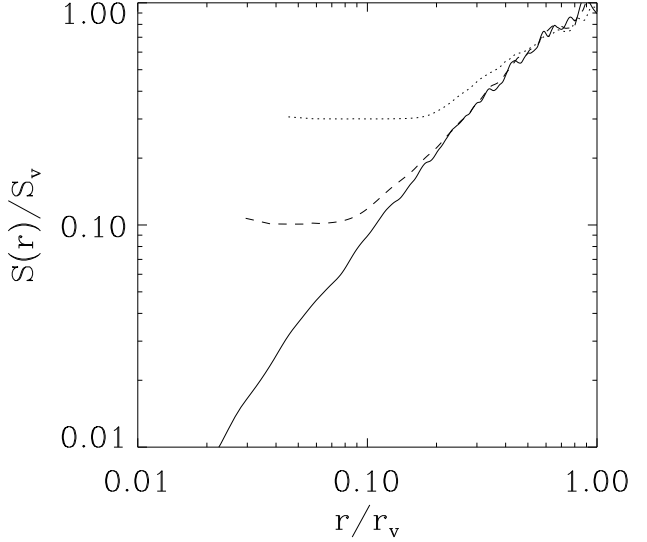


**Figure 3.** The entropy profiles in two preheating models: the dotted line corresponds to  $S_{\text{ph}} = 0.3 S_v$  and the dashed line corresponds to  $S_{\text{ph}} = 0.1 S_v$ , compared to the model without preheating (solid line). We ignore radiative cooling.

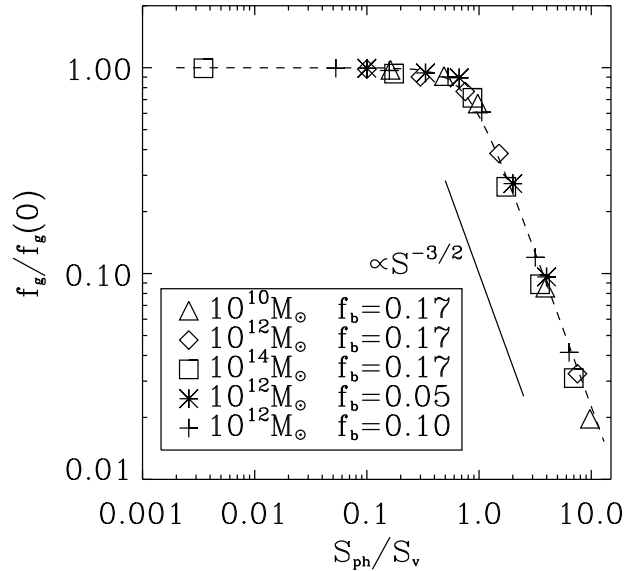


**Figure 4.** The gas fraction that can be accreted into a halo in the presence of preheating, normalized by the fraction in the absence of preheating, as a function of normalized preheating entropy,  $S_{\text{ph}}/S_v$ . Different symbols represent simulations with various halo masses and baryon fractions, as indicated in the panel. The dashed curve corresponds to equation (38), while the solid line corresponds to the scaling relation,  $\propto S_{\text{ph}}^{-3/2}$ .

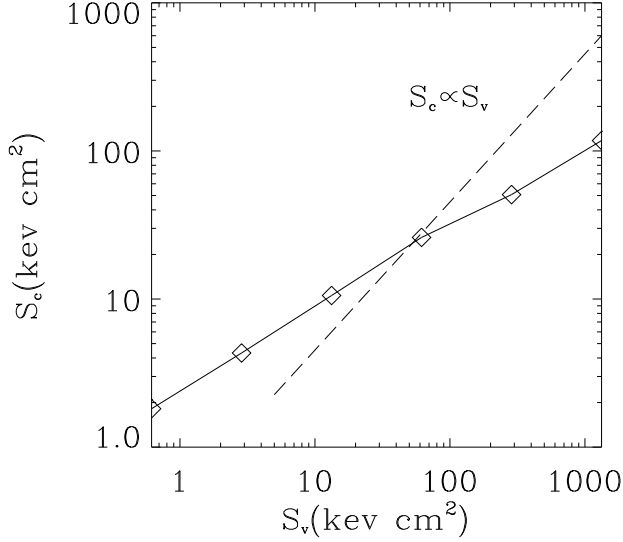


**Figure 6.** The critical entropy  $S_c$ , as defined in the text, versus halo virial entropy  $S_v$ . The dashed line shows  $S_c \propto S_v$ .

$M_{\text{acc}}(S_{\text{ph}})$ , respectively. The corresponding quantities in the non-preheating cases are denoted by  $M_{\text{cool}}(0)$  and  $M_{\text{acc}}(0)$ . Figure 5 shows the ratio  $f_{\text{cool}}(S_{\text{ph}}) \equiv M_{\text{cool}}(S_{\text{ph}})/M_{\text{acc}}(0)$  and  $f_{\text{acc}}(S_{\text{ph}}) \equiv M_{\text{acc}}(S_{\text{ph}})/M_{\text{acc}}(0)$  as a function of the preheating entropy,  $S_{\text{ph}}$ , for halos of different masses. As one can see, the behavior of  $f_{\text{cool}}(S_{\text{ph}})$  is quite different for different mass halos. In massive halos, the accreted gas fraction decreases slowly with increasing amount of preheating entropy, while the cold gas fraction drops rapidly. Thus, in these systems, a large amount of the accreted gas stays in the hot phase. The situation is quite different for low mass halos, where almost all of the accreted gas can cool even if the IGM is preheated.

To quantify the importance of preheating on gas cooling, we define a “critical” specific entropy  $S_c$  by

$$f_{\text{cool}}(S_c)/f_{\text{cool}}(0) = 1/2, \quad (39)$$

where  $f_{\text{cool}}(S)$  is the fraction of the gas that can cool in a halo if the IGM is preheated to a specific entropy  $S$ . Figure 6 shows the  $S_c - S_v$  relation obtained from our simulations. Clearly, one needs a higher initial entropy to prevent the accreted gas from cooling in more massive systems. However, the critical specific entropy,  $S_c$ , does not increase as fast as  $S_v$ : the logarithmic slope of the  $S_c - S_v$  relation is approximately 2/3 not 1. Thus, if there were a mechanism that could preheat the gas associated with halos to an initial specific entropy that was proportional to  $S_v$ , the effect on gas cooling would be more important for more massive systems. On the other hand, if the IGM were everywhere preheated to the same level of specific entropy, then the effect would be more important for lower-mass systems.

It is also interesting to look at how preheating affects the gas cooling rate as a function of time. Since preheating flattens the gas density distribution, the time scale for gas cooling is similar over a large range of radii. This is different from the case without preheating, where the cool-

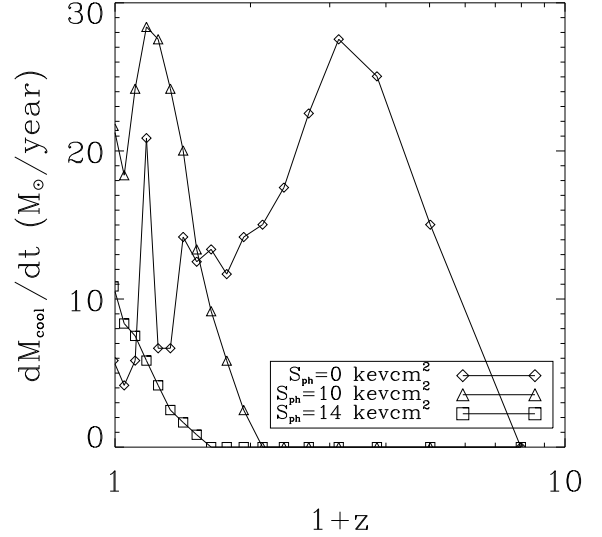


**Figure 7.** The gas cooling rates in a  $10^{12} h^{-1} M_{\odot}$  halo versus redshift. Different symbols represent results for different preheating levels, as indicated in the panel.

ing time scale is shorter in the inner, denser regions and the cooling proceeds in an inside-out fashion. In Figure 7, we show the cooling rate as a function of redshift in a halo of  $10^{12} h^{-1} M_{\odot}$ . Here we consider two models of preheating, one with  $S_{\text{ph}} = 10 \text{ keV cm}^2$  and the other with  $S_{\text{ph}} = 14 \text{ keV cm}^2$ , and compare the results of these two models to the case with  $S_{\text{ph}} = 0$ . Again, we assume the accreted gas has a single phase. As one can see, preheating causes a delay in gas cooling. The cooling rate peaks at  $z \sim 2$  in the absence of preheating, and the cooling rate at the present time is about  $4 M_{\odot}/\text{year}$ . Preheating decreases the cooling rate at high  $z$  but enhances the cooling rate at lower  $z$ , because much of the gas has to wait until a later time before it can cool. For all the simulations we analyzed, the delay in gas cooling is more important if the ratio  $S_{\text{ph}}/S_v$  is larger.

Based on the results presented above, one can conclude that the accretion of cold gas into galaxies occurs rather late in the presence of preheating. This may be a problem, because it implies that most of the stars in present spiral galaxies must form very late. As we will see below, this problem can be alleviated by assuming that the gas is in a multi-phase rather than in a single-phase state.

## 4.2 Cooling in multi-phase media

There are many reasons to believe that the gas in galaxy halos has a multi-phase structure. First of all, at the temperatures considered here, the gas is expected to be thermally unstable, and so a multi-phase medium can develop through thermal instability (Field 1965; Fall & Rees 1985; Murray & Lin 1990). Secondly, the density field of the CDM universe is expected to be clumpy, which can promote thermal instability. The development of a multi-phase medium will affect the cooling of the halo gas, as the cooling time in the high-

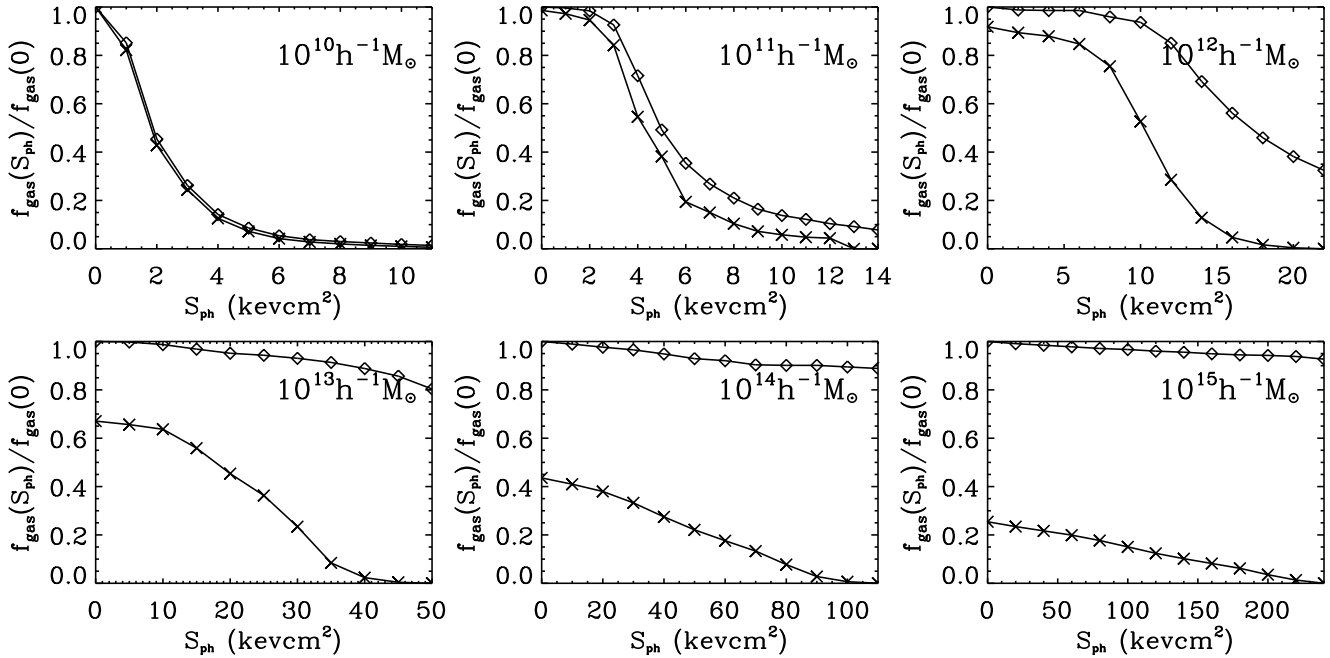


**Figure 5.** Diamonds show the amount of accreted gas in the presence of preheating, normalized by the amount of accreted gas in the absence of preheating, versus the preheating entropy. Crosses show the amount of cold gas, normalized by the amount of accreted gas in the absence of preheating, versus the preheating entropy. Different panels show results for halos of different masses.

density/low-temperature phase may become shorter than the age, even if the single-phase cooling time does not. In this section, we use simple models to demonstrate how gas cools in a multi-phase medium.

To incorporate a multi-phase medium in our simulations, we split each gas shell into  $N$  phases over a range of gas densities. The gas in each phase is assumed to move with its host shell and to be in pressure equilibrium with the other phases in any subsequent evolution. Each sub-shell, which represents gas in a phase, is characterized by its number density  $n_{ij}$ , temperature  $T_{ij}$  and mass  $m_{ij}$ , where  $i$  labels a shell, and  $j$  labels a sub-shell phase. The thermodynamics of the multi-phase gas is treated in the same way as that described in Thomas (1988). At each time step, the radiative cooling of every sub-shell is calculated using its current density and temperature, and a new density and a new temperature are determined through the hydrodynamical equations (see Thomas 1988 and its appendix for details). Once the temperature of a sub-shell drops below  $10^4$  K, this phase drops out of the shell, and the gas in the sub-shell is then deposited into a central disk that is assumed to form at the center of the host halo. The remaining phases in the shell are assumed to expand adiabatically to occupy the extra volume. In practice, we adopt the multi-phase model for a gas shell as soon as it is accreted within the current virial radius. We, therefore, neglect the details of how a multi-phase medium actually develops.

The density distribution of the multi-phase gas is described by the volume fraction function,  $f(\rho, \bar{\rho})d\rho$ , which describes the volume fraction occupied by a phase with a density in the range  $\rho \pm d\rho/2$  for a gas shell with mean density  $\bar{\rho}$ . By definition  $\int f d\rho = 1$ . In our simulations, each gas shell initially contains 50 sub-shells equally spaced in

$\log \rho$ . Since the form of  $f(\rho, \bar{\rho})$  is not known *a priori*, we consider three simple models, as examples, which are plotted in Figure 8. Two of these are log-normal functions with two different widths,  $\sigma_{\log \rho/\rho_0} = 0.15$  and  $0.05$ , where  $\rho_0$  is the median density of the distribution, related to the mean density,  $\bar{\rho}$ , by  $\rho_0 = \bar{\rho}e^{-\sigma^2/2}$ . In the third model, the volume-fraction function is assumed to have the ‘‘cooling tail’’ form,

$$f(\rho, \bar{\rho}) \propto \rho^{-(4-\alpha)} \exp[-(\bar{\rho}/\rho)^{2-\alpha}], \quad (40)$$

where  $\alpha$  is the slope of the cooling function,  $\Lambda \propto T^\alpha$ . This model has been used to describe multi-phase cooling flows in galaxy clusters (Nulsen 1986; Thomas 1988; Waxman & Miralda-Escudé 1995). We have adopted  $\alpha = 0.4$ , which roughly describes the cooling by free-free process. In the simulations, we only sample phases with  $f > 10^{-5}$ . Our test with the ‘‘cooling tail’’ model shows that our simulation reproduces the results obtained by Thomas (1988).

To demonstrate the effect of changing the gas from a single-phase medium to a multi-phase medium, we consider a case where the final halo mass is  $10^{12} h^{-1} M_\odot$ , and the initial preheating entropy  $S_{\text{ph}} = 10 \text{ keV cm}^2$ , using the three models for  $f$  described above. Figure 9 shows the gas cooling histories, i.e. the mass of cooled gas as a function of redshift, compared to that of a single-phase model. As expected, the cooling history is more extended in models where the density distribution is broader. For a broader density distribution, there is larger amount of high-density gas that can cool rapidly. If the density distribution is as broad as the ‘‘cooling-tail’’ model, cold gas can be assembled into galaxies much earlier than in the single-phase model.

Remember that in the single-phase model, cooling is inside-out. So if the cooling time of the gas were comparable to the age, only gas in the innermost region could cool. On



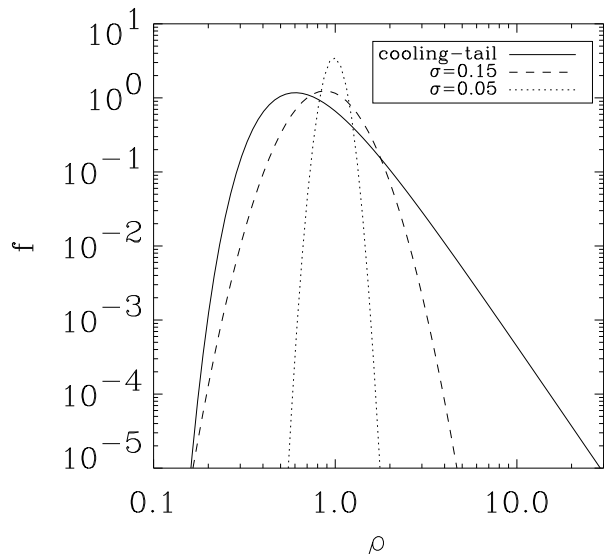


**Figure 8.** The volume fraction occupied by phases of different density. The dotted and dashed curves are log-normal distributions with dispersions  $\sigma_{\log \rho/\rho_0} = 0.05$  and  $0.15$ , respectively. The solid curve is the “cooling tail” model described in the text. The x-axis is scaled by the mean density,  $\bar{\rho}$ .

the other hand, in a multi-phase medium, cooling can occur almost everywhere in the high-density phases. To demonstrate this, we plot in Figure 10 the initial (Lagrangian) radii that contain 20%, 50% and 80% of the gas that drops out to the cold phase in a time interval  $\Delta t = 0.5$  Gyrs as a function of  $(1+z)$ . In the single-phase case, all the gas within a certain Lagrangian radius can cool, and so the 20%, 50% and 80% radii are all the same (the dashed curve in Figure 10). For the single-phase case shown in Figure 10, this “cooling radius” is much smaller than the virial radius of the halo (dot-dashed curve), implying that only gas in the innermost parts of the halo can cool. In the multi-phase case, however, at any time gas can cool to the cold phase over a large range of Lagrangian radii. This result could have important implications for the formation of galaxy disks. *N*-body simulations show that the specific angular momentum of dark matter particles increases roughly linearly with the Lagrangian radius (Bullock 2001). Thus, if the angular momentum of the gas follows that of dark matter, the specific angular momentum of the cooled gas in the single-phase case is expected to be lower than the average specific angular momentum of the dark matter, since only the gas in the inner regions can cool. This could lead to the formation of galaxy disks that are too compact (e.g. Mo, Mao & White 1998). On the other hand, in the multi-phase model, the cold gas that settles into the disk comes from various radii, and so its average specific angular momentum may be comparable to that of the dark matter, a condition that is required to reproduce the observed sizes of galaxy disks (e.g. Mo, Mao & White 1998).

As demonstrated in Figure 11, if the initial specific entropy,  $S_{\text{ph}}$ , is comparable to or smaller than the critical value,  $S_c$ , the total amount of gas that can cool at the

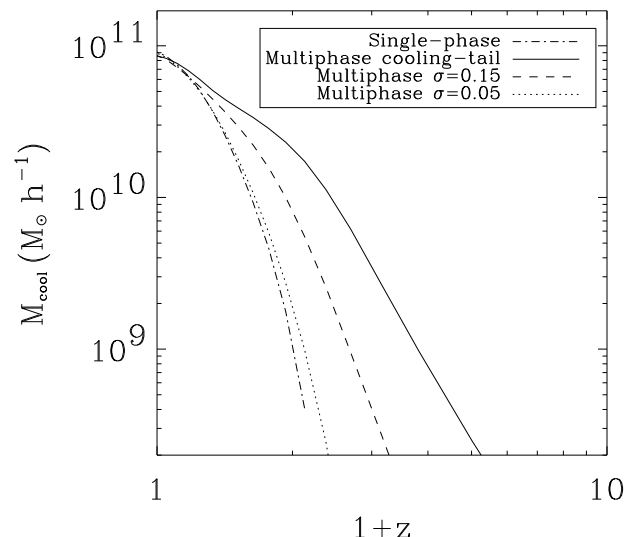


**Figure 9.** The total amount of cooled gas in a  $10^{12} h^{-1} M_{\odot}$  halo with preheating entropy  $S_{\text{ph}} = S_c \sim 10 \text{ keV cm}^2$ . The dash-dotted line shows the result of a model that assumes the halo gas is a single-phase medium. The three other curves show the results of the three multi-phase models: the cooling-tail model (solid curve), the log-normal model with  $\sigma = 0.15$  (dashed curve), and log-normal model with  $\sigma = 0.05$  (dotted curve).

present time is quite insensitive to the assumed gas density distribution, although different models of the gas density distribution produce different accretion histories of cold gas. This occurs because the cooling time of the gas accreted into halos, even when it is assumed to be in a single-phase, is comparable to or shorter than the age of the universe at the present time. However, if the value of  $S_{\text{ph}}$  is much larger than  $S_c$ , the total amount of gas that cools by the present time can be significantly larger in the multi-phase model than in the single-phase model, for halos with masses  $\gtrsim 10^{11} h^{-1} M_{\odot}$ . For halos with smaller masses, cooling is so effective that almost all the accreted gas can cool even if  $S_{\text{ph}} > S_c$ .

## 5 APPLICATIONS

So far we have discussed in general how preheating affects gas accretion and cooling in dark matter halos. In the present section, we consider two specific examples that may be relevant to the actual formation of galaxies.

### 5.1 Preheating by a central AGN

First, we consider the case where the gas associated with a dark halo is heated by the outflow of a central AGN. Recent observations show that almost all galaxies, at least those with a significant spheroidal component, i.e. elliptical galaxies and spiral galaxies with a significant bulge, host a central supermassive black hole (SBH) with a mass that is correlated with the velocity dispersion of the bulge,

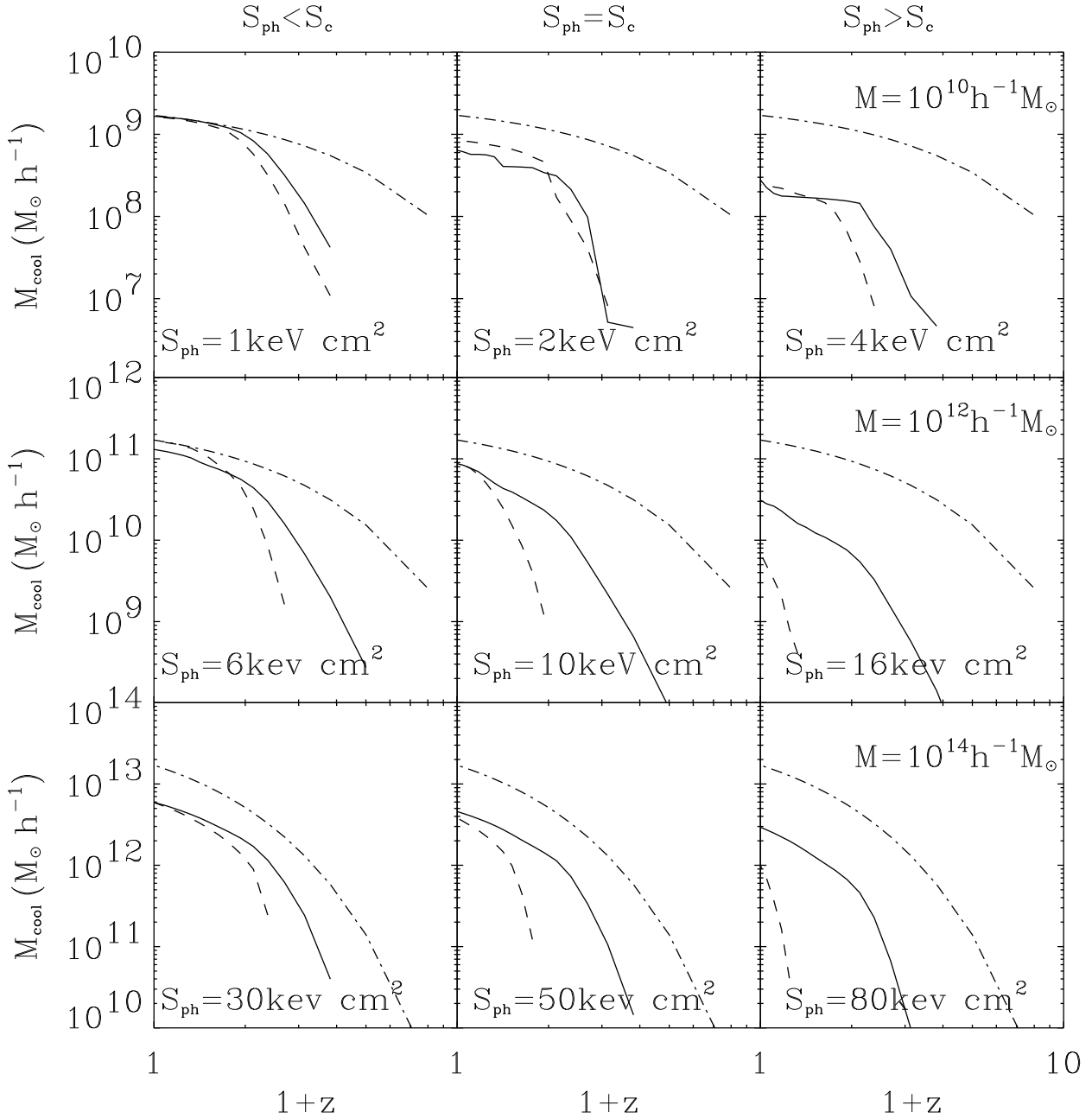


**Figure 11.** The mass of cooled gas as a function of redshift. In each panel, the solid curve shows cooled gas mass in a simulation assuming a multi-phase medium with the “cooling tail” density distribution, and the dashed curve stands for the result of the corresponding single-phase simulation. The dash-dotted curve shows the baryon fraction ( $f_b = 0.17$ ) times the halo mass. Results are shown for halos of different present masses which are noted in the right column panels for each row and different preheating entropies which are noted at the bottom of each panel.

$M_{\text{BH}} = 10^{8.3} M_{\odot} (\sigma/200 \text{ km s}^{-1})^{4.02}$  (Tremaine et al. 2002). This correlation is quite independent of redshift out to  $z \approx 3$  (Sheilds et al. 2003). If fed with gas, these black holes are able to power AGNs that may produce outflows and heat the gas in dark matter halos. This kind of feedback process has been suggested as a plausible mechanism to quench both star formation and black halo growth in massive galaxies (Binney & Tabor 1995; Silk & Rees 1998; Nulsen & Fabian 2000; Springel et al. 2005). However, it is still unclear how

the energy associated with the AGNs is coupled to the gas, allowing it to quench gas cooling and star formation. It has been suggested that the energy deposition is localized so that the outflows driven by AGNs are thermalized in the ambient medium only within the host galaxy (e.g. Springel et al. 2005). However, recent numerical simulations with jets show that the jet may tunnel through low-density regions of the ambient medium, and that the energy may be easily carried to large distances and thermalized there (Vernaleo

Based on the above discussion, we write

$$S_{\text{ph}} = S_{\text{ph},12} \frac{S_{\text{v}}}{S_{\text{v},12}}, \quad (41)$$

where  $S_{\text{v},12}$  is the virial entropy of a  $10^{12} h^{-1} M_{\odot}$  halo and  $S_{\text{ph},12}$  is a normalization factor, taken to be the value of  $S_{\text{ph}}$  corresponding to that in a halo of present mass  $M = 10^{12} h^{-1} M_{\odot}$ . To estimate the normalization factor, we use the model presented in Scannapieco & Oh (2004). Since the lifetime of an AGN is typically  $\sim 10^7$  years, much shorter than a Hubble time, the effect of an AGN on gas at large distances may be modeled as a blast wave. Adopting the Sedov-Taylor solution, we can write the postshock entropy as

$$S_{\text{s}} = 1.8 \times 10^4 \text{ keV cm}^2 E_{60} \delta_{\text{s}}^{-5/3} (1+z)^{-5} R_{\text{s,Mpc}}^{-3}, \quad (42)$$

where  $E_{60}$  is the kinetic energy in an AGN outflow,  $E$ , in units of  $10^{60}$  ergs,  $\delta_{\text{s}}$  is the overdensity of the surrounding medium defined as  $\delta_{\text{s}} = \rho_{\text{b}}/\bar{\rho}_{\text{b}}$ , and  $R_{\text{s,Mpc}}$  is the shock radius in Mpc and is given by the Sedov solution as

$$R_{\text{s}} = 1.7 \text{ Mpc } E_{60}^{1/5} \delta_{\text{s}}^{-1/5} (1+z)^{-3/5} t_{\text{Gyr}}^{2/5}, \quad (43)$$

with  $t_{\text{Gyr}}$ , the evolution time of the shock in gigayears. Following Scannapieco & Oh (2004), we assume that  $E$  is a constant fraction of the bolometric luminosity,  $L_{\text{bol}}$ :  $E \approx \epsilon_{\text{k}} L_{\text{bol}} t_{\text{AGN}}$ , where we take  $\epsilon_{\text{k}} \sim 0.05$ . The AGN life time,  $t_{\text{AGN}}$ , is assumed to be proportional to the dynamical time of a virialized halo, and is approximated by  $t_{\text{AGN}} \approx 5.2 \times 10^7 \text{ yr } (1+z)^{-3/2}$  (e.g. Barkana & Loeb 2001). We assume the bolometric luminosity related to the luminosity in the blue band,  $L_{\text{bol}} = 10.4 L_{\text{B}}$ , as suggested by observations (Elvis et al. 1994). Assuming that an AGN shines at its Eddington luminosity, one can relate the B-band luminosity to the mass of the black hole ( $M_{\text{BH}}$ ) as  $L_{\text{Edd,B}} = 5.73 \times 10^3 L_{\odot} M_{\odot}^{-1} M_{\text{BH}}$  (e.g. Willott, McLure & Jarvis 2003). We use the observed relation between  $M_{\text{BH}}$  and the circular velocity  $v_{\text{c}}$  obtained by Ferrarese et al. (2002),

$$M_{\text{BH}} = 1.4 \times 10^8 M_{\odot} F \left( \frac{v_{\text{c}}}{300 \text{ km s}^{-1}} \right)^5, \quad (44)$$

to estimate the black hole mass, where  $F$  is a model parameter taken to be 0.6, as in Wyithe & Loeb (2003). With all these assumptions, one can estimate  $S_{\text{ph},12} \sim 7 \text{ keV cm}^2$  at  $z = 2$ , assuming  $\delta_{\text{s}} = 1$ .

We first carry out single-phase simulations similar to those presented in Section 4, but with the preheating entropy set by (41) with  $S_{\text{ph},12} = 7 \text{ keV cm}^2$ . For comparison, we also consider another sequence with  $S_{\text{ph},12} = 3.5 \text{ keV cm}^2$ . Figure 12 shows the mass of cooled gas at  $z = 0$  as a function of halo mass. It is clear that the suppression of gas cooling by AGN preheating is more important in more massive halos. This result can be understood using Figure 6. Since the AGN preheating entropy considered here is proportional to the virial entropy of the halo, the effect of preheating is more important in more massive halos. In this model, there is an upper-mass limit for the cooled gas mass, which is about  $\sim 3 \times 10^{11} h^{-1} M_{\odot}$  assuming  $S_{\text{ph},12} = 7 \text{ keV cm}^2$ , and about  $\sim 2 \times 10^{12} h^{-1} M_{\odot}$  assuming  $S_{\text{ph},12} = 3.5 \text{ keV cm}^2$ . This maximum mass occurs at a halo mass of  $M \sim 4 \times 10^{12}$  for  $S_{\text{ph},12} = 7 \text{ keV cm}^2$ , and at  $M \sim 5 \times 10^{13}$  for  $S_{\text{ph},12} = 3.5 \text{ keV cm}^2$ . Thus, for a given preheating amplitude  $S_{\text{ph},12}$ , significant gas cooling in halos

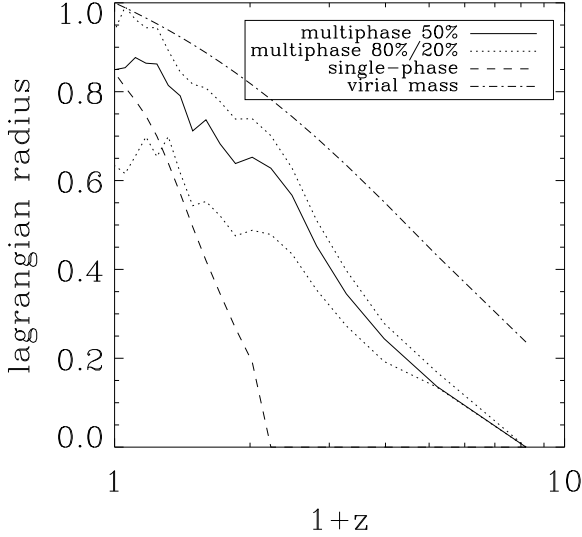


**Figure 10.** The Lagrangian radius of the gas shell that cools as a function of redshift normalized to the present time ( $z = 0$ ). Results are shown for a  $10^{12} h^{-1} M_{\odot}$  halo with preheating entropy  $S_{\text{ph}} = S_{\text{c}} = 10 \text{ keV cm}^2$ , and the “cooling-tail” model is adopted for the multi-phase medium. The solid curve shows the Lagrangian radius within which 50% of the cooled gas is contained at each redshift, while the two dotted curves mark the radii which contain 20% and 80% of the cooled gas. For comparison, the dashed curve shows a model in which the medium is assumed to be single-phase. The dot-dashed curve is the Lagrangian radius of the forming halo.

& Reynolds 2005). Without going into details, we consider a simple model here.

We assume that the energy injected by an AGN is proportional to the mass of the SBH,  $E_{\text{AGN}} \propto M_{\text{BH}}$ . Observations of spiral galaxies with SBHs show that the mass of the SBH is tightly correlated with the circular velocity of the galaxy,  $M_{\text{BH}} \propto v_{\text{c}}^5$  (Ferrarese 2002). Since  $v_{\text{c}}$  is related to the virial mass of the spiral galaxy’s host halo,  $M \propto v_{\text{c}}^3$ , we have  $E_{\text{AGN}}/M \propto v_{\text{c}}^2$ . Thus, if the energy of the AGN is to heat all the gas associated with its host halo, the energy gained by each particle from the AGN feedback is roughly proportional to  $v_{\text{c}}^2$ , i.e. to the virial temperature of the host halo. If such feedback occurs at the same redshift for systems with different masses, the specific entropy owing to AGN preheating is expected to be proportional to the virial entropy of the halo, i.e.  $S_{\text{ph}} \propto S_{\text{v}}$  (Scannapieco & Oh 2004). However, observations of quasars suggest that there is an upper limit to quasar luminosities (Fan et al. 2003), corresponding to a SMB mass of  $M_{\text{BH}} \sim 10^9 M_{\odot}$ . This mass corresponds to  $v_{\text{c}} = 500 \text{ km s}^{-1}$  assuming Eddington luminosities and the observed  $M_{\text{BH}} - v_{\text{c}}$  relation (Wyithe & Loeb 2003). Such a limit in  $M_{\text{BH}}$  implies that the  $M_{\text{BH}} - v_{\text{c}}$  relation must be broken for massive halos. There must be some process that quenches the growth of the SMB and, given the  $M_{\text{BH}} - \sigma$  relation, also the growth of the central galaxy in massive halos. In what follows, we will consider a preheating model with  $S_{\text{ph}} \propto S_{\text{v}}$ , and examine if the observed mass limit can be accommodated.

above a certain mass can only occur in progenitors before the formation of the central AGN. As soon as the central AGN has formed, gas cooling is effectively suppressed by preheating.

This result has significant implications. Observations of AGNs suggest that there is an upper limit for quasar luminosity (Fan et al. 2003), which corresponds to a black hole with a mass of  $\sim 10^9 M_\odot$  assuming it radiates with an Eddington luminosity. This mass is approximately equal to that of the central black hole in a halo with a circular velocity  $v_c \sim 470 \text{ km s}^{-1}$  (corresponding to a halo mass of  $10^{13.5} M_\odot$  at the present time), using the observed  $M_{\text{BH}} - v_c$  relation (Wyithe & Loeb 2003). If the mass of a central black hole scales with its host halo as the  $M_{\text{BH}} - v_c$  relation for all dark matter halos, such an upper limit for black hole mass would not be expected. Thus, there must be a process that can prevent the growth of central black holes in massive halos. The AGN preheating model considered here may alleviate this difficulty. Before the formation of the supermassive black hole, gas can cool effectively and the mass of the central black hole grows rapidly. However, as soon as the mass of the central black hole reaches a value of  $\sim 10^9 M_\odot$ , gas cooling is effectively suppressed and the black hole stops growing. The same process also prevents the growth of the central galaxy, so that the 1-d velocity dispersion of the central galaxy cannot be much larger than  $330 \text{ km s}^{-1}$ . This may explain why not many galaxies can have velocity dispersions much larger than this (e.g. Sheth et al. 2003).

There are, however, a number of uncertainties in this conclusion. First of all, if the growth of black hole mass is indeed saturated at a fixed value, the preheating produced by the AGN would become unimportant as the dark matter halo grows and the corresponding  $S_v$  becomes larger than the entropy generated by the AGN. Cooling will then resume in halos with  $v_c \gg 330 \text{ km s}^{-1}$ . To prevent further cooling in massive halos after the formation of SMBs, one may still need energy sources to balance the radiative cooling. One possibility here is the feedback from the central galaxy in ‘‘radio’’ mode. Although the energy feedback in such a mode is much weaker than that in the ‘‘quasar’’ mode, it may be sufficient to balance radiative cooling in massive halos (e.g. Croton et al. 2006). Another uncertainty is the possible development of a multi-phase medium in massive halos, which may promote additional radiative cooling. To demonstrate this, we run multi-phase simulations, assuming the ‘‘cooling tail’’ model, for halos more massive than  $10^{12} h^{-1} M_\odot$ . The dashed curves in Figure 12 show the mass of cooled gas at  $z = 0$  as a function of halo mass for this model. Now, there is no sharp truncation in the cold gas mass, although the total cold gas mass is still reduced relative to the non-preheating model. Unfortunately, it is unclear whether a significant multi-phase medium can develop in massive halos. Indeed, in order for the ‘radio-mode’ feedback to work in massive halos, the formation of multi-phase media has to be suppressed.

## 5.2 Low-mass halos in a warm intergalactic medium

As one can see from Figure 12, AGN preheating has little effect on small halos, because the black holes in these systems are small and the cooling is efficient. Thus, AGN preheating

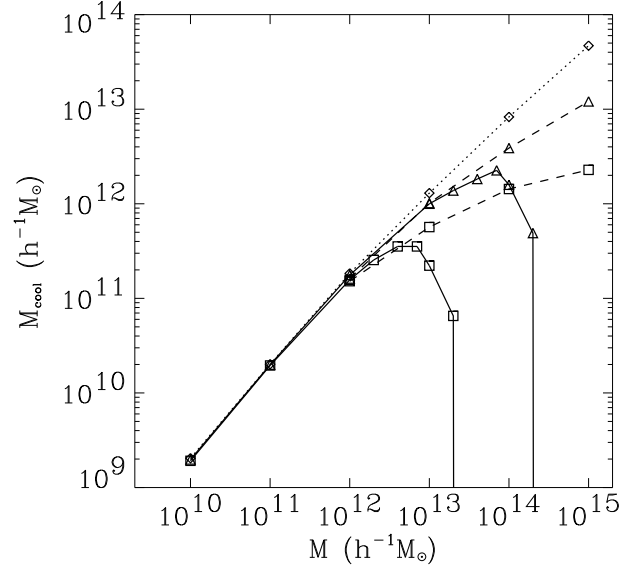


**Figure 12.** Cooled gas mass versus halo mass in simulations assuming AGN preheating. The squares show results assuming  $S_{\text{ph},12} = 7 \text{ keV cm}^2$ , and the triangles show results assuming  $S_{\text{ph},12} = 3.5 \text{ keV cm}^2$ . Symbols connected by solid lines are results assuming a single-phase medium, and symbols connected by dashed curves are results assuming the ‘‘cooling tail’’ model of the multi-phase medium. For comparison, diamonds connected by dotted lines are the results assuming no preheating.

cannot suppress star formation in low-mass halos to explain the flat faint-end slope of the galaxy luminosity function. Some other processes must be at work in small halos. In this subsection, we consider a model in which all small halos ( $M < 10^{12} M_\odot$ ) are assumed to be embedded in a warm medium with an initial specific entropy  $S_{\text{ph}} \sim 10 \text{ keV cm}^2$ . This model is motivated by the proposal of Mo et al. (2005) that low-mass halos at low redshift may be surrounded by a warm intergalactic medium produced by gravitational pancaking. Another possibility for such preheating is supernova explosions associated with the formation of halo stars, bulge stars, and stars in the thick disk.

We consider a case where  $S_{\text{ph}} = 8 \text{ keV cm}^2$ . Since such a low value of  $S_{\text{ph}}$  has little effect on halos with  $M > 10^{12} M_\odot$ , we concentrate on smaller halos. Figure 13 shows the mass of cooled gas,  $M_{\text{cool}}$ , as a function of halo mass. For low mass halos,  $M_{\text{cool}}$  scales with halo mass roughly as  $M^2$ . This can be understood as follows. As we have seen in Section 3, if  $S_{\text{ph}} \geq S_v$ , as is the case for low-mass halos, the fraction of accreted gas scales as  $f_{\text{acc}} = (S_{\text{ph}}/S_v)^{-3/2}$ . Since at a fixed redshift  $S_v \propto T_v$  and  $T_v \propto M^{2/3}$ , the mass of the accreted gas  $M_{\text{acc}} = f_{\text{acc}} f_b M \propto M^2$  for a constant preheating entropy. In small halos almost all the accreted gas can cool, so we have  $M_{\text{cool}} \propto M^2$ . This result supports the assumption made by Mo et al. (2005) about the  $M_{\text{cool}} - M$  relation for low-mass halos accreting gas in a medium preheated by the formation of pancakes. As shown in Mo et al. (2005), such a  $M_{\text{cool}} - M$  relation is required to explain both the faint-end slope of the galaxy luminosity function and the HI-mass function of galaxies. It should be noted that

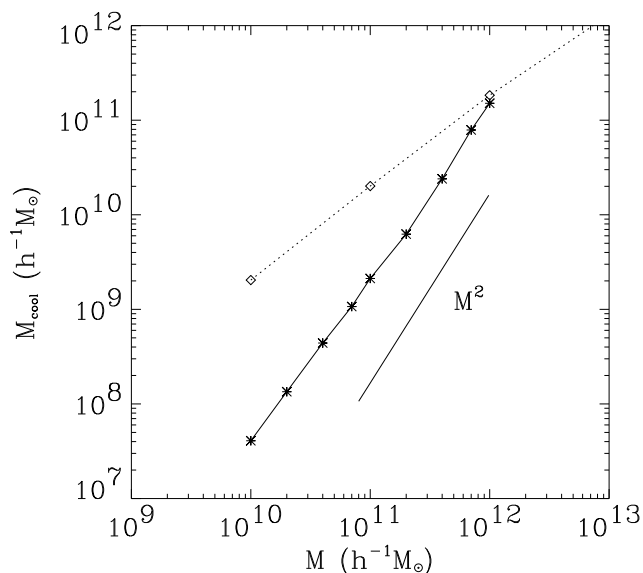


**Figure 13.** The mass of cooled gas versus halo mass for a model in which the intergalactic gas is preheated to a specific entropy  $S_{\text{ph}} = 8.0 \text{ keV cm}^{-2}$  (stars). In this case, the cooled gas mass scales with halo mass roughly as  $M^2$ . For comparison, the diamonds show the results for a model without preheating.

the multi-phase model does not change the cold gas mass in these halos. As we have demonstrated in Section 4, the cooling is always efficient in small halos. Hence, once the gas is accreted into low-mass halos, it can cool no matter it was in high-density or low-density phases. Note, however, that the assembly history of the cold gas into the central disk may depend significantly on whether the medium is single-phase or multi-phase, as discussed in Section 4.2.

## 6 SUMMARY

In this paper, we examine the effects of preheating on gas cooling and accretion into dark matter halos, using a 1-D hydrodynamical code and realistic halo formation histories. We explore the behavior of the preheated gas by varying the virial mass of the halo and the amount of preheating. We find that preheating can both prevent gas accretion into dark matter halos and reduce the radiative cooling of that gas. If the preheating entropy is larger than the virial entropy of the halo, the fraction of the gas that can be accreted into a halo scales roughly as  $f_g \propto (S_{\text{ph}}/S_v)^{-3/2}$ . For low-mass halos, almost all the accreted gas can cool, and so preheating reduces the total amount of cold gas that can be assembled into the central galaxy only by reducing the total amount of gas that can be accreted by the halo. For massive halos, on the other hand, preheating not only reduces the amount of gas that can be accreted, but also suppresses radiative cooling. We also examine the effects of a multi-phase medium on the cooling of halo gas and find that the cooling history of multi-phase gas is very different from that of a single-phase medium model. In a multi-phase medium, gas cooling can occur in the dense phases soon after the

gas is accreted into the halo, in contrast to a single-phase medium where gas cooling is delayed. Also, in a single-phase medium, gas cooling in general proceeds in an inside-out fashion, while in a multi-phase medium gas can cool, at a given time, over a wide range of radii.

We consider two examples where preheating may have played important roles in galaxy formation and evolution. First, we examine a case where the gas associated with a dark matter halo is preheated by an AGN outflow powered by a central supermassive black hole. Using assumptions made in recent quasar feedback models, we demonstrate that such preheating can effectively suppress gas cooling in halos with masses above  $\sim 10^{13} h^{-1} M_{\odot}$ , leading to an upper mass limit of about  $10^{12} h^{-1} M_{\odot}$  for the central galaxy that can form in such a massive halo. This may be the reason why the galaxy luminosity (mass) function has a sharp break at the bright (massive) end. This suppression of gas cooling in massive halos may also be responsible for the observed bimodality in the colour-magnitude diagram. Observations show that the blue sequence, which consists of galaxies with significant star formation, is truncated at the bright end, with very few blue galaxies having stellar masses exceeding  $10^{11} M_{\odot}$ . The more massive galaxies are all red, with little current star formation. This suggests that there must be some process to quench star formation in these massive galaxies. Recent semi-analytical models of galaxy formation including AGN feedback show that the bimodality in the colour distribution and the truncation of the blue sequence can be reproduced if the feedback from the central galaxy is in the “radio mode” (e.g. Croton et al 2005; Cattaneo et al 2006). However, in order for the “radio-mode” feedback to be effective, the halo gas must be in a diffuse hot form. In the scenario we consider here, the halo gas is preheated by the feedback from the central AGN in the “quasar mode”, and any subsequent cooling is suppressed in the preheated medium. This may help create the hot diffuse halos within which the “radio mode” feedback can act effectively.

The second example we consider is the case where the intergalactic medium is assumed to be preheated to a constant entropy level. This model is motivated by the scenario outlined in Mo et al. (2005) where such preheating may help explain the observed stellar- and HI-mass functions of galaxies at the low-mass end in current CDM models. Our simulations confirm that such preheating can indeed produce the cold-gas-mass/halo-mass relation,  $M_{\text{cool}} \propto M^2$ , as is required to match the observed stellar- and HI-mass functions in the current CDM theory.

The results obtained in this paper demonstrate that preheating may have played an important role in galaxy formation. To explore the observational consequences of the preheating scenario, one needs to combine the results obtained here with the dark matter halo population predicted by current CDM models of structure formation, to quantify how preheating affects the properties of the galaxy population and of the intergalactic medium. The best approach is perhaps through semi-analytic modeling, and we plan to do this in a future paper.

## ACKNOWLEDGMENT

We thank David Weinberg and Anne Thoul for providing their 1-d hydrodynamical code that helped the development of the code used in this paper. We thank Neal Katz for reading the manuscript and many beneficial comments. We thank Avi Loeb for useful discussion. HJM would like to acknowledge the support of NSF AST-0607535, NASA AISR-126270 and NSF IIS-0611948.

## REFERENCES

- Barkana R., Loeb A., 2001, *Phys. Rep.*, 349, 125  
 Bertschinger E., 1983, *ApJ*, 268, 17  
 Binney J.J., 1977, *ApJ*, 215, 483  
 Binney J., Tabor G., 1995, *MNRAS*, 276, 663  
 Bond J.R., Cole S., Efstathiou G., Kaiser N., 1991, *ApJ*, 379, 440  
 Bowers R.L., Wilson J.R., 1991, *Numerical Modeling in Applied Physics and Astrophysics*  
 Bullock J.S., Dekel A., Kolatt T.S., Kravtsov A.V., Klypin A.A., Porciani C., Primack J.R., 2001, *ApJ*, 555, 240  
 Cattaneo A., Dekel A., Devriendt J., Guiderdoni B., Blaizot J., 2006, *MNRAS*, 370, 1651  
 Cen R., Ostriker J.P., 1992, *ApJ*, 393, 22  
 Croton D.J., Springel V., White S.D.M., De Lucia G., Frenk C.S., Gao L., Jenkins A., Kauffmann G., Navarro J.F., Yoshida N., 2006, *MNRAS*, 365, 11  
 Dijkstra M., Haiman Z., Rees M.J., Weinberg D.H., 2004, *ApJ*, 601, 666  
 Elvis M., Wilkes B.J., McDowell J.C., Green R.F., Bechtold J., Willner S.P., Oey M.S., Polowski E., Cutri R., 1994, *ApJS*, 95, 1  
 Fall S.M., Rees M.J., 1985, *ApJ*, 298, 18  
 Fan X. et al. , 2003, *AJ*, 125, 1649  
 Ferrarese L., 2002, *ApJ*, 578, 90  
 Field G.B., 1965, *ApJ*, 142, 531  
 Gnedin N.Y., 2000, *ApJ*, 542, 535  
 Hoefl M., Yepes G., Gottlöber S., Springel V., 2006, *MNRAS*, 371, 401  
 Jing Y.P., Suto Y., 2000, *ApJ*, 529, 69  
 Katz N., Gunn J.E., 1991, *ApJ*, 377, 365  
 Katz N., Weinberg D.H., Hernquist L., 1996, *ApJSS*, 105, 19  
 Lu Y., Mo H.J., Katz N., Weinberg M.D., 2006, *MNRAS*, 368, 1931  
 Mac Low M.-M., Ferrara A., 1999, *ApJ*, 513, 142  
 Mo H.J., Mao S., 2002, *MNRAS*, 333, 768  
 Mo H.J., Mao S., White S.D.M., 1998, *MNRAS*, 295, 319  
 Mo H.J., Yang X., van den Bosch F.C., Katz N., 2005, *MNRAS*, 363, 1155  
 Moore B., Governato F., Quinn T., Stadel J., Lake G., 1998, *ApJ*, 499, L5  
 Murray S.D., Lin D.N.C., 1990, *ApJ*, 363, 50  
 Navarro J.F., Frenk C.S., White S.D.M., 1996, *ApJ*, 462, 563  
 Navarro J.F., Frenk C.S., White S.D.M., 1997, *ApJ*, 490, 493  
 Nulsen P.E.J., 1986, *MNRAS*, 221, 377  
 Nulsen P.E.J., Fabian A.C., 2000, *MNRAS*, 311, 346  
 Oh S.P., Benson A.J., 2003, *MNRAS*, 342, 664  
 Piffaretti R., Jetzer P., Kaastra J.S., Tamura T., 2005, *A&A*, 433, 101  
 Press W.H., Schechter P., 1974, *ApJ*, 187, 425  
 Quinn T., Katz N., Efstathiou G., 1996, *MNRAS*, 278, 49  
 Richtmyer R.D., Morton K.W., 1967, *Difference Methods for Initial Value Problems*, Second edn. Interscience, New York  
 Rees M. J., Ostriker J.P., 1977, *MNRAS*, 179, 541  
 Scannapieco E., Oh S. P., 2004, *ApJ*, 608, 62  
 Shields G.A., Gebhardt K., Salviander S., Wills B.J., Xie B., Brotherton M.S., Yuan J., Dietrich M., 2003, *ApJ*, 583, 124  
 Sheth R.K., Mo H.J., Tormen G., 2001, *MNRAS*, 323, 1  
 Sheth R. K., et al. , 2003, *ApJ*, 594, 225  
 Silk J.I., 1977, *ApJ*, 211, 638  
 Silk J., Rees M.J., 1998, *A&A*, 331, 1  
 Springel V., Di Matteo T., Hernquist L., 2005, *MNRAS*, 361, 776  
 Springel V., Hernquist L., 2003, *MNRAS*, 339, 289  
 Strickland D.K., Stevens I.R., 2000, *MNRAS*, 314, 511  
 Thomas P., 1988, *MNRAS*, 235, 315  
 Thoul A., Weinberg D.H., 1995, *ApJ*, 442, 480  
 Tozzi P., Norman C., 2001, *ApJ*, 546, 63  
 Tremaine S., et al. , 2002, *ApJ*, 574, 740  
 van den Bosch F.C., Abel T., Hernquist L., 2003, *MNRAS*, 346, 177  
 Vernaleo J.C., Reynolds C.S., 2006, *ApJ*, 645, 83  
 Waxman E., Miralda-Escudé J., 1995, *ApJ*, 451, 451  
 Wechsler R.H., Bullock J.S., Primack J.R., Kravtsov A.V., Dekel A., 2002, *ApJ*, 568, 52  
 White S.D.M., Frenk C.S., 1991, *ApJ*, 379, 52  
 White S.D.M., Rees M.J., 1978, *MNRAS*, 183, 341  
 Willott C.J., McLure R.J., Jarvis M.J., 2003, *ApJ*, 587, 15  
 Wyithe J.S.B., Loeb A., 2003, *ApJ*, 595, 614  
 Yang X., Mo H.J., van den Bosch F.C., 2003, *MNRAS*, 339, 1057  
 Yang X., Mo H.J., Jing Y.P., van den Bosch F.C., 2005, *MNRAS*, 358, 217  
 Zhao D.H., Mo H.J., Jing Y.P., Börner G., 2003a, *MNRAS*, 339, 12  
 Zhao D.H., Jing Y.P., Mo H.J., Börner G., 2003b, *ApJ*, 597, L9